Deployment and Calibration of Reference Reflectance Tarps for Use with Airborne Imaging Sensors

M. Susan Moran, Ross B. Bryant, Thomas R. Clarke, and Jiaguo Qi

Abstract

Chemically treated canvas tarps of large dimension (8 by 8 m) can be deployed within the field of view of airborne digital sensors to provide a stable ground reference for converting image digital number (DN) to surface reflectance factor (ρ). However, the accuracy of such tarp-based conversion is dependent upon a good knowledge of tarp ρ at a variety of solar and view angles (θ_s and θ_v), and upon good care and proper deployment of tarps. In this study, a set of tarps of ρ ranging from 0.04 to 0.64 were evaluated to determine the magnitude of error in measured tarp ρ associated with variations in θ_s, θ_v, and for reasonable levels of tarp dirtiness. Results showed that, for operational values of θ_s and θ_v and for reasonable levels of tarp dirtiness, the variation of measured tarp ρ from the factory-designated ρ could easily be greater than 50 percent. On the other hand, we found that, if tarps were deployed correctly and kept clean through careful use and periodic cleaning, and if tarp ρ was determined through calibration equations that account for both θ_s and θ_v, the greatest sources of error were minimized. General calibration equations were derived and provided here; these will be useful for applications with tarps of the same factory-designated ρ values as those used in this study. Furthermore, equations were provided to allow calibration coefficients to be determined from the value of factory-designated ρ for the visible and near-infrared spectral bands. The major limitation of tarps as calibration sources was related to the difficulty associated with deploying heavy, cumbersome tarps under normal field conditions characterized by moderate wind, dust, heat, and possibly mud. This study should provide tarp users with the information necessary to properly deploy tarps and process results for accurate image interpretation.

Introduction

With recent advances in multispectral video and digital imaging sensors, there has been a surge in commercial companies offering aircraft-based, spectrally filtered, visible and near-infrared (NIR) digital images to agricultural customers. These products become far more valuable if the digital numbers (DN) can be converted to a value that is independent of atmospheric and insolation variations, and is thus comparable over time for monitoring seasonal crop and soil conditions. The reflectance factor (the ratio of reflected and incident radiation at the surface) is such a value, and has become the basic measurement required for most remote sensing algorithms and models. One approach for converting DN to values of surface reflectance factor (ρ) has been to derive a linear regression equation between DN and ρ, based on targets of known ρ within the flight line of the airborne sensors. Chemically treated canvas tarps of large dimensions (8 m by 8 m) have been used to provide the stable ground references needed for this approach (Teillet *et al.*, 1987; O'Neill *et al.*, 1997). Such tarps are commercially available with stipulations of ρ ranging from 0.02 to 0.80 and ρ stability through the visible and NIR spectrum.

Several issues must be addressed for proper deployment of such tarps. First, the calibration provided by commercial producers is a directional/hemispherical calibration measured with an integrating-sphere spectrophotometer system such as that described by Zerlaut and Anderson (1981). In the nomenclature of Hsia and Weidner (1981), the directional/hemispherical reflectance factor would be designated by $\rho(0°/h)$, where the first parenthetical term refers to the view angle of the radiometer (where a view normal to the target is 0°) and the second term refers to the light source angle (where irradiance from a hemisphere is termed h). There is ample evidence (e.g., Jackson *et al.*, 1987) that $\rho(0°/h)$ differs from the reflectance factor measured in field conditions with the sun as the illumination source, termed directional/directional reflectance factor or $\rho(0°/\theta_s)$, where θ_s is the solar zenith angle. Because of its dependence on incidence angle, $\rho(0°/\theta_s)$ is considerably more sensitive to the non-Lambertian properties of the reference tarp than is $\rho(0°/h)$. Thus, a calibration equation for field deployment of such tarps must be derived as a function of solar zenith angle. Furthermore, this calibration equation must account for variations in the view angle of the sensor (θ_v), where the directional/directional reflectance factor is $\rho(\theta_v/\theta_s)$. Finally, once these equations are derived, their effectiveness under long term field conditions must be evaluated.

In this report, we addressed the issues of tarp directional/directional calibration, and the change in tarp properties with long term field deployment. Swatches from several tarps of $\rho(0°/h) = 0.04, 0.08, 0.32, 0.48$, and 0.64 were calibrated using a goniometer and the field techniques described by Jackson *et al.* (1987; 1992), resulting in polynomial equations relating swatch $\rho(0°/\theta_s)$ to solar zenith angle for each spectral band.

M.S. Moran and R.B. Bryant are with the USDA Agricultural Research Service, Southwest Watershed Research Center, 2000 E. Allen Rd., Tucson, AZ 85719 (moran@tucson.ars.ag.gov).

T.R. Clark is with the USDA Agricultural Research Service, U.S. Water Conservation Laboratory, 4331 E. Broadway Rd., Phoenix, AZ 85040.

J. Qi is with the Department of Geography, Michigan State University, 416 Natural Sciences Building, East Lansing, MI 48824-1115.

Photogrammetric Engineering & Remote Sensing
Vol. 67, No. 3, March 2001, pp. 273–286.

0099-1112/01/6703–273$3.00/0

These equations were used to evaluate the non-lambertian properties of the tarps over the visible, NIR, and shortwave IR (SWIR) spectrum, and to determine if general calibration equations could be derived for universal application.

The variation in $\rho(\theta_v/\theta_s)$ due to sensor viewing angle (θ_v) was measured for tarps of $\rho(0°/h) = 0.04, 0.08, 0.48$, and 0.64 over a range of θ_v from $-55°$ to $+55°$. These measurements were used to model the bidirectional reflectance factor distribution function (BRDF) of the tarps and provide a simple correction equation to account for effects of both θ_v and θ_s.

In collaboration with a private company, RESOURCE21[1] (R21, Englewood, Colorado), we evaluated nine sets of tarps of varying condition, each set consisting of tarps of $\rho(0°/h) = 0.04$, 0.08, 0.48, and 0.64 (i.e., 36 sample tarps of 8 by 8 meters). This collection of tarps allowed us to validate the goniometer-derived calibration equations and determine if calibration adjustments needed to be made for physical changes in the tarps over time.

Materials and Methods

The tarps used in this analysis were manufactured by Tracor GIE (Austin, Texas). Tracor GIE supplies tarps of two substrate materials: woven polyester and spun bonded non-woven polyester (referred to herein as woven and non-woven materials, respectively). The woven material is heavier, more durable, and more expensive than the non-woven material, where the latter has an expected life span of 90 deployments. The non-woven material is offered by Tracor GIE to negate the need for constant calibration checks and repairs; that is, the tarp can be economically replaced with a new tarp before the occurrence of material or chemical degradation. To attain the specified $\rho(0°/h)$ characteristics, both woven and non-woven tarps are treated with a pigment of titanium dioxide and carbon black, and coated with a pigmented acrylic resin.

The following sections cover the methods used in (1) tarp calibration related to θ_s, (2) evaluation of tarp temporal degradation, and (3) tarp calibration related to θ_v.

Tarp Calibration Related to θ_s

In 1995, scientists at several U.S. Department of Agriculture (USDA) and University locations acquired a set of 12 8- by 8-m woven reference tarps with a variety of $\rho(0°/h)$ values from Tracor GIE. One tarp ($\rho(0°/h) = 0.32$) was also chemically treated to provide a constant emissivity over the spectral range 8 to 12 μm. In 1997, we obtained the 36 non-woven tarps from R21 (referred to above) which were originally produced by Tracor GIE and had $\rho(0°/h)$ values of 0.04, 0.08, 0.48, and 0.64. With each tarp, Tracor GIE provided a 0.7- by 1.4-m swatch of the same material treated in the same chemical solutions for calibration purposes. Each swatch was then cut to a size of 0.7 m by 0.7 m and stapled to a 0.7- by 0.7-m plywood board (of 6 mm thickness) that had been painted (three coats) with a flat black paint. These board-mounted swatches were the right size for comparison with reference panels of known $\rho(0°/\theta_s)$ and for use with the field goniometer.

The field goniometer used for this study was the same as that used by Jackson *et al.* (1987; 1992). The goniometer provides a calibration based on conditions similar to those encountered in the field; that is, the sun and sky are the sources of irradiance and the calibration measurements are made with the same radiometer and data logger used for subsequent field measurements (Walter-Shea *et al.*, 1993). The procedures for goniometer measurements and data processing were in strict accordance with the procedures outlined by Jackson *et al.* (1987; 1992) and Walter-Shea and Biehl (1990). All swatches were cross-referenced to a sintered polytetrafluorethylene (trade name Spectralon) reference panel provided by Labsphere (North Sutton, New Hampshire) which had been calibrated to a pressed halon standard in 1991 by Jackson *et al.* (1992) and then stored until it was used for this calibration. For each swatch, voltages were measured with a Modular Multispectral Radiometer (MMR) at seven solar incidence angles (15°, 19.4°, 29°, 39.2°, 48.8°, 58.8°, and 67.9°). The MMR was filtered to six spectral bands, similar to several of the Landsat Thematic Mapper (TM) spectral bands: (b1) 0.45 to 0.52 μm; (b2) 0.52 to 0.60 μm; (b3) 0.63 to 0.69 μm; (b4) 0.76 to 0.90 μm; (b5) 1.15 to 1.30 μm; and (b6) 1.55 to 1.75 μm.

In accordance with suggestions by Jackson *et al.* (1992), we fit a quadratic equation through the voltage/solar zenith angle data at four angles (15°, 19.4°, 29°, and 39.2°) and used that to predict a voltage value at 10°. With the cross-reference to the calibrated Spectralon panel and the goniometer information of spectral voltages at eight solar zenith angles, we derived fourth-order polynomial relations between $\rho(0°/\theta_s)$ and solar zenith angles from 10 to 68° for the swatches (for each of i spectral bands), where

$$\rho(0°/\theta_s)_i = a_{0,i} + a_{1,i}\theta_s + a_{2,i}\theta_s^2 + a_{3,i}\theta_s^3 + a_{4,i}\theta_s^4. \quad (1)$$

The order of the polynomial was selected to allow comparison with the fourth-order polynomials derived by Jackson *et al.* (1992) for Spectralon panels.

Goniometer-based calibrations were conducted on two dates in 1995 and 1997. In 1995, we calibrated ten swatches of the woven tarps of $\rho(0°/h) = 0.04, 0.08, 0.32$, and 0.48; in 1997, we calibrated four swatches of non-woven tarps of $\rho(0°/h) = 0.04, 0.08, 0.48$, and 0.64; and we repeated the calibrations of four selected woven tarps of $\rho(0°/h) = 0.04, 0.08, 0.32$, and 0.48.[2] During the two years between calibrations, the woven swatches were stored in a cool, dry room within a dark box to minimize surface degradation. The two calibrations were designed to determine calibration equations for the multiple woven and non-woven swatches, and to quantify temporal tarp degradation by repeating calibrations of selected swatches.

Tarp Temporal Degradation

The physical changes of tarp $\rho(0°/\theta_s)$ over time was evaluated based on the 36 non-woven, 8- by 8-m tarps deployed by R21 during the crop growing season in 1997 (April through October). In support of bi-weekly aircraft overpasses, R21 deployed these tarps sets (of $\rho(0°/h) = 0.04, 0.08, 0.48$, and 0.64) at locations in Texas, Nebraska, Iowa, California, and Alberta, Canada. At the end of the season, these tarps were delivered to our location in Arizona for post-season calibration. Because the tarps were of size 8 m by 8 m, it was impossible to use the goniometer for calibration. Instead, we laid the tarps out in a strategic configuration to allow rapid measurements with a yoke-based spectral radiometer at a variety of θ_s.

The tarps were split into three groups of 12 tarps each. Each tarp was folded in half with the bottom side up, and piled one

[1]The use of company names and brand names are necessary to report factually on available data; however, the USDA neither guarantees nor warrants the standard of the product, and the use of the name by USDA implies no approval of the product to the exclusion of others that may also be suitable.

[2]Woven swatches were designated by the value of $\rho(0°/h)$ followed by a letter to discriminate swatches of the same $\rho(0°/h)$ (e.g., the three woven swatches $\rho(0°/h) = 0.04$ were designated 0.04a, 0.04b, and 0.04c). Non-woven swatches were designated by the value of $\rho(0°/h)$ followed by "n" for non-woven (e.g., the non-woven swatch of $\rho(0°/h) = 0.04$ was designated 0.04n).

on top of the other in three side-by-side piles. Then, one-by-one, the top side of the tarp was exposed by peeling back a section of size 2 m by 8 m. This allowed the operators carrying a yoke-mounted Exotech to measure $\rho(0°/\theta_s)$ of three tarps along a single transect. The Exotech is a radiometer with filters similar to the MMR except that it does not include the SWIR bands. The measurements of $\rho(0°/\theta_s)$ made with the MMR and Exotech were in close agreement (differences less than 0.01 $\rho(0°/\theta_s)$ in all bands), so we considered the readings interchangeable.

After each tarp was measured, the underlying tarp was exposed to allow the yoke operators to repeat the transect and measure $\rho(0°/\theta_s)$ of the next three tarps. With this configuration, it was possible to measure $\rho(0°/\theta_s)$ of all 36 tarps within a 20-minute period. On the measurement day, the weather was excellent for data collection all day; there were no clouds in sight and the sky was bright blue. We repeated the yoke measurements at three solar zenith angles: 39°, 51°, and 59°. Measurements of a 0.6- by 0.6-m Spectralon reference panel were made every five minutes through the tarp measurements.

It was visually apparent that the R21 tarps were in different stages of dirtiness due to different conditions at the five field locations. To record these differences, a team of three scientists made a visual estimate of tarp *dirtiness*, and classified the tarps into four subjective classes: clean, somewhat dirty, dirty, and very dirty. These classes were used in the subsequent analysis to explain differences in tarp $\rho(0°/\theta_s)$.

We conducted an additional experiment designed specifically to address the issues of tarp dirtiness. We again mounted the swatches of the tarps of $\rho(0°/h) = 0.04, 0.08, 0.48$, and 0.64 on painted boards, and used the MMR and the goniometer to measure $\rho(0°/\theta_s)$ of the swatches at four solar zenith angles (15°, 29°, 49°, and 68°). This process was repeated for clean swatches and for dirty swatches. The "clean" swatches were simply the swatches that we received from Tracor GIE which had been stored in a cool, dark closet for the past year. After goniometer measurements were made on the clean swatches, we scattered one handful of dry soil on each swatch; we rubbed the soil into the swatch with a cotton rag (to simulate a dirty tarp that had been folded repeatedly); and then we brushed it off again, producing the "dirty" swatch. Subsequently, a set of goniometer measurements was made of these swatches at four solar zenith angles.

This experiment resulted in measurements of MMR voltage at four solar zenith angles for swatches of both levels of cleanliness. According to the technique described by Jackson *et al.* (1987; 1992), we subtracted the voltage associated with the varying diffuse radiation (measured using a sun shade) from the total voltage measured. Then, we divided the voltage by $\cos(\theta_s)$ to obtain comparable voltage measurements for determining the percentage change in tarp $\rho(0°/\theta_s)$ due to dirtiness.

Tarp Calibration Related to θ_v

Several R21 tarps were used to evaluate the influence of varying θ_v on the tarp $\rho(\theta_v/\theta_s)$. This was accomplished by mounting an Exotech radiometer on an apparatus designed at the USDA-ARS Water Conservation Laboratory to measure $\rho(\theta_v/\theta_s)$ (Jackson *et al.*, 1990). The radiometer, when looking at nadir view, is 2.5 m above the tarp. The apparatus has a movable arm that allows the sensor to be positioned at different view angles. Attached to the radiometer was a clinometer to automatically record the view angles. By different alignment of the apparatus base, the tarps could be scanned from different directions (along the principle plane of the sun, 45° off principal plane, and 90° off principal plane) at different solar angles. The nadir view angle measurements could then be compared with the yoke-based measurements for validation.

Measurements of $\rho(\theta_v/\theta_s)$ were made over four tarps of $\rho(0°/h) = 0.04, 0.08, 0.48$, and 0.64 at two solar zenith angles, viewing angles from +55° to −55°, and three scanning planes. This experiment was conducted in a large parking lot with three small but bright buildings on the north side and a big Quonset hut to the south. These surroundings may have affected the $\rho(\theta_v/\theta_s)$ measurements made in the 90° viewing plane due to reflected radiance from the buildings; thus, measurements made in that plane were not used in the subsequent BRDF model inversion.

Results

Similar to the Materials and Methods Section, results are presented in three parts covering tarp calibration related to θ_s, tarp temporal degradation, and tarp calibration related to θ_v.

Tarp Calibration Related to θ_s

The tarp calibration related to changing θ_s was conducted exclusively with tarp swatches using the field goniometer. Results include a validation of the method, an evaluation of tarp response, the derivation of a "general" calibration equation, and a comparison of calibrations for woven and non-woven tarp swatches.

Calibration of the Reference Spectralon Panel Measured in 1991 and 1995

The goniometer measurements provided a relation for each swatch between the voltage (V) measured by the radiometer and a range of solar zenith angles. In order to obtain $\rho(0°/\theta_s)$ from $V(0°/\theta_s)$, it was necessary to cross-calibrate each swatch with a panel of known $\rho(\theta_v/\theta_s)$ (see Walter-Shea and Biehl (1990), Appendix 1). In works by Jackson *et al.* (1987; 1992), Spectralon panels were calibrated with reference to a pressed halon standard and found to have stable values of $\rho(0°/\theta_s)$ over time. So, rather than use a pressed halon standard which is difficult and expensive to prepare, for this calibration we used a Spectralon panel that had been calibrated in 1991 by Jackson *et al.* (1992) and carefully stored for this purpose.

To assure that the Spectralon calibration from 1991 had not changed appreciably, we measured the non-lambertian characteristics of the Spectralon panel during the 1995 goniometer study. Fourth-order polynomials were derived from the voltages measured at seven solar zenith angles (15° to 68°) for the two goniometer runs. To compare the shapes of relations measured in 1995 to the shape of the relation obtained in 1991 for the Spectralon panel, we computed the ratio of $\rho(0°/45°)_{1991}$ and $V(0°/45°)_{1995}$ for each band, and multiplied the polynomial coefficients of the 1995 calibration equations by this value to obtain equations which produced identical values of $\rho(0°/45°)$. For all bands, the mean absolute difference between the 1995 normalized voltage and the 1991 $\rho(0°/\theta_s)$ was less than 0.005. With this indirect validation, we assumed that it was proper to use the Spectralon panel for cross-calibration in the 1995 and 1997 studies, with the 1991 Spectralon calibration equation.

Goniometer-Based Calibration of Woven Swatches

For woven swatches of $\rho(0°/h) > 0.08$, we computed fourth-order absolute calibration equations using eight solar zenith angles (10° to 68°) for the six spectral bands. For woven swatches of $\rho(0°/h) \leq 0.08$, the signal-to-noise ratio was low for large solar zenith angles, so fourth-order equations were fit using six solar zenith angles (10° to 50°). In all cases, the r^2 values of the regression equations were greater than 0.99. The results for woven swatches of several $\rho(0°/h)$ values covering spectral bands from 0.45 to 1.75 μm (MMR b1 to b6) are presented in Figure 1. All swatches exhibited substantial non-lambertian behavior over the range of solar zenith angles from 10 to 70°. Furthermore, the absolute values of $\rho(0°/\theta_s)$ and the non-lambertian characteristics of the SWIR spectral bands b5 and b6 were substantially different from those of the visible and near-infrared spectral bands b1 to b4.

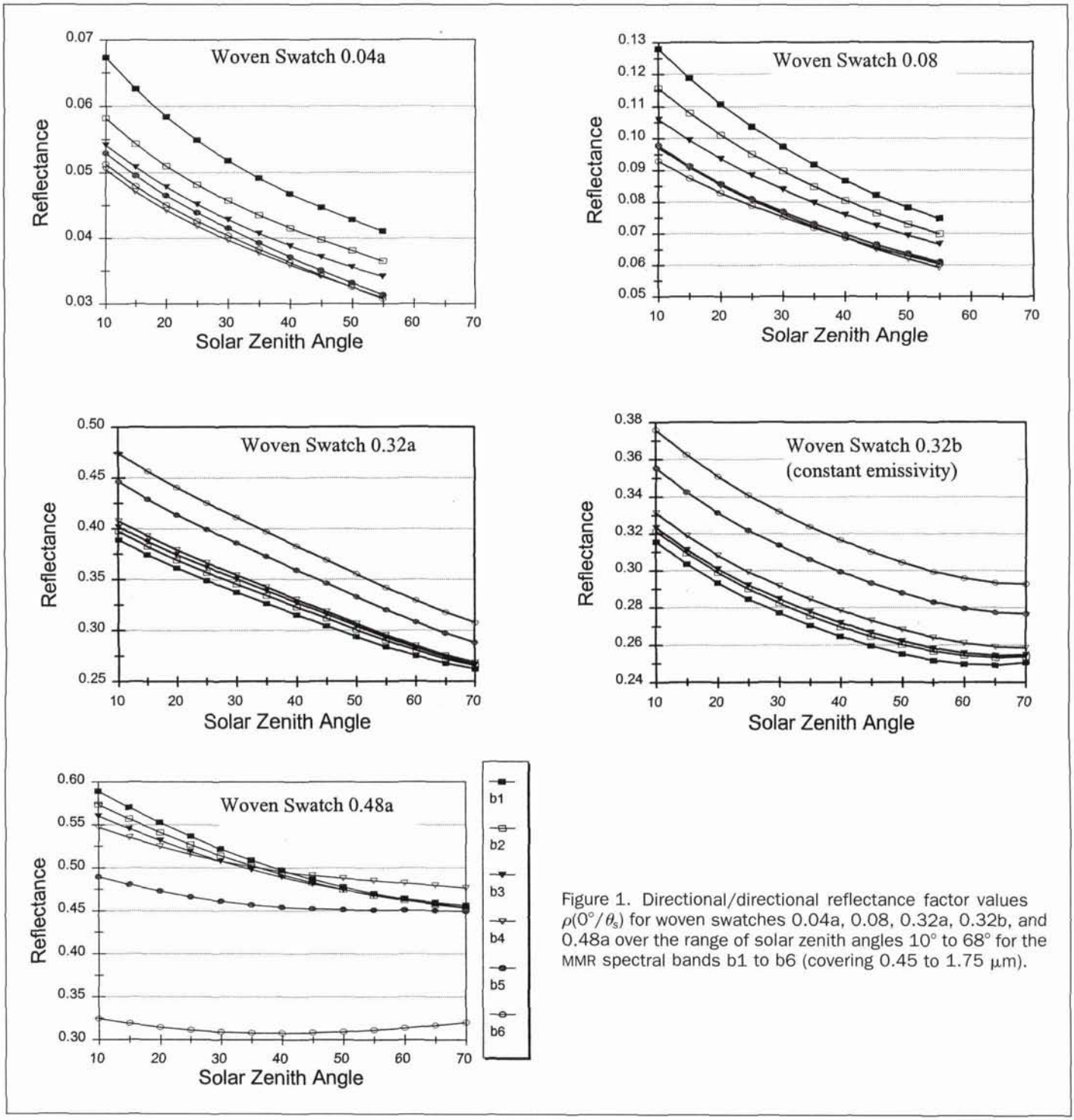

Figure 1. Directional/directional reflectance factor values $\rho(0°/\theta_s)$ for woven swatches 0.04a, 0.08, 0.32a, 0.32b, and 0.48a over the range of solar zenith angles 10° to 68° for the MMR spectral bands b1 to b6 (covering 0.45 to 1.75 μm).

It is notable that, for b1 to b4, $\rho(0°/45°)$ was close to Tracor-specified values of $\rho(0°/h)$ whereas, for b5 and b6, the difference between $\rho(0°/45°)$ and $\rho(0°/h)$ was a function of $\rho(0°/h)$. That is, for the SWIR spectral bands, the value of $\rho(0°/45°)$ deviated substantially from $\rho(0°/h)$, and the magnitude and direction of the variation appeared to be related to the SWIR wavelength and value of $\rho(0°/h)$. Results presented in Figure 1 showed that swatch 0.32b (the swatch chemically treated for the property of constant emissivity) had different $\rho(0°/\theta_s)$ properties from those of swatch 0.32a, though both swatches had Tracor calibration of $\rho(0°/h) = 0.32$. This may have been due to the "sparkly" appearance of swatch 0.32b in the sunlight, which may have resulted in some specular reflectance from the treated surface.

The "shapes" of the calibration equations differed by band and by value of $\rho(0°/h)$, and in units of absolute $\rho(0°/\theta_s)$, the swatches of lower $\rho(0°/h)$ had flatter shapes. To analyze the shape of the relation between $\rho(0°/\theta_s)$ and θ_s independently of $\rho(0°/h)$, the curves for all bands of each swatch were normalized by adjusting the intercept (a_0) to force a value of 1.0 at $\theta_s = 45°$. Two trends were apparent (Figure 2). First, the greatest relative non-lambertian properties were associated with the swatches of lowest $\rho(0°/h)$. For swatches of $\rho(0°/h) = 0.04$, the $\rho(0°/10°)$ was nearly 1.6 times $\rho(0°/45°)$. Second, the widening of the set of lines as angles

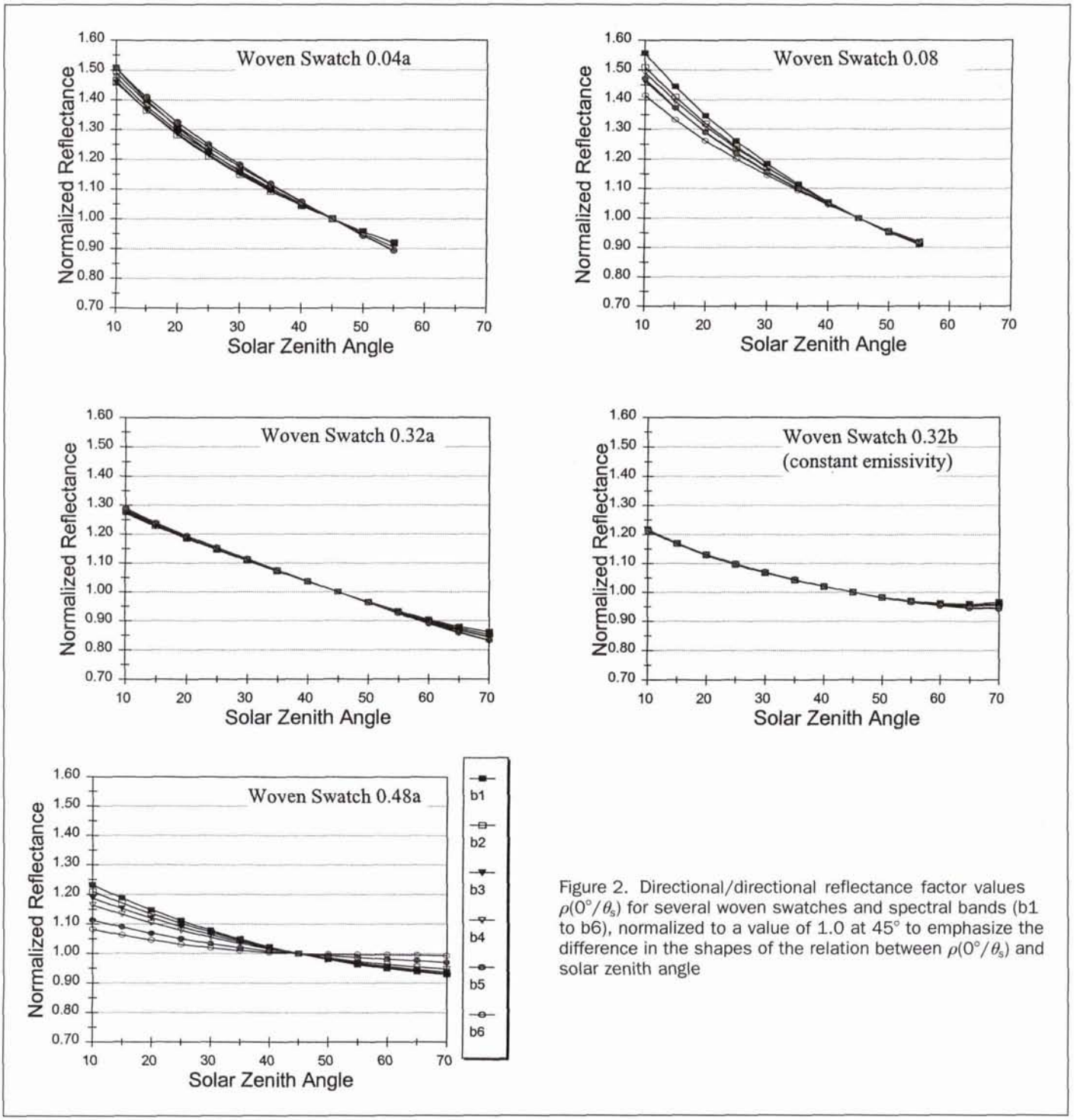

Figure 2. Directional/directional reflectance factor values $\rho(0°/\theta_s)$ for several woven swatches and spectral bands (b1 to b6), normalized to a value of 1.0 at 45° to emphasize the difference in the shapes of the relation between $\rho(0°/\theta_s)$ and solar zenith angle

deviated from 45° indicated that non-lambertian characteristics were different for different bands. The degree of "widening" differed by swatch, where the non-lambertian properties of swatches of $\rho(0°/h) = 0.32$ were uniform across all bands and those of swatches of $\rho(0°/h) = 0.48$ were non-uniform.

Derivation of General Tarp Calibration Equations for Woven Swatches

Because we had three swatches of $\rho(0°/h) = 0.04$ and four swatches of $\rho(0°/h) = 0.48$, it was possible to explore the potential for "general" calibration equations that could be applied to other tarps produced by Tracor GIE under well-controlled, reproducible conditions. The $\rho(0°/\theta_s)$ for each band for swatches of the same $\rho(0°/h)$ were relatively similar. The mean absolute difference (MAD) between $\rho(0°/\theta_s)$ of swatch 0.04a and that of swatches 0.04b and 0.04c (all $\rho(0°/h) = 0.04$) was less than 0.006 for b1 to b4 and nearly 0.01 for b5 and b6. The average MAD between $\rho(0°/\theta_s)$ of swatch 0.48a and that of swatches 0.48b to 0.48d (all $\rho(0°/h) = 0.48$) was less than 0.025 for b1 to b4 and nearly 0.04 for b5 and b6. Because this variation in $\rho(0°/\theta_s)$ was far less than the variation associated with the non-lambertian behavior of the swatches (Figure 1), we felt justified in suggesting general equations for tarps of the four $\rho(0°/h)$ values measured in this study.

TABLE 1. POLYNOMIAL EQUATIONS RELATING $\rho(0°/\theta_s)$ AND θ_s FOR WOVEN SWATCHES OF $\rho(0°/h)$ = 0.04, 0.08, 0.32, 0.32+, AND 0.48; WHERE $\rho(0°/\theta_s) = a_{0,i} + a_{1,i}\,\theta_s + a_{2,i}\theta_s^2 + a_{3,i}\theta_s^3 + a_{4,i}\theta_s^4$, AND b1 TO b6 ARE THE MMR SPECTRAL WAVELENGTH BANDS IN THE VISIBLE, NIR, AND SWIR SPECTRUM.

$\rho(0°/h)$ = 0.04	$a_{0,i}$	$a_{1,i}$	$a_{2,i}$	$a_{3,i}$	$a_{4,i}$
b1	0.082	−1.359E−03	1.911E−05	−1.954E−07	1.089E−09
b2	0.072	−1.089E−03	1.450E−05	−1.512E−07	8.803E−10
b3	0.065	−9.211E−04	1.103E−05	−1.134E−07	7.266E−10
b4	0.064	−9.954E−04	1.556E−05	−2.109E−07	1.369E−09
b5	0.067	−1.038E−03	1.683E−05	−2.505E−07	1.681E−09
b6	0.067	−1.175E−03	2.587E−05	−4.348E−07	2.908E−09
$\rho(0°/h)$ = 0.08					
b1	0.151	−2.727E−03	4.403E−05	−5.367E−07	3.225E−09
b2	0.135	−2.273E−03	3.703E−05	−4.76 E−07	2.957E−09
b3	0.123	−1.960E−03	3.297E−05	−4.439E−07	2.835E−09
b4	0.114	−2.026E−03	4.032E−05	−6.126E−07	4.019E−09
b5	0.116	−2.166E−03	4.487E−05	−6.444E−07	3.939E−09
b6	0.108	−1.785E−03	3.800E−05	−5.972E−07	3.881E−09
$\rho(0°/h)$ = 0.32					
b1	0.427	−4.347E−03	7.708E−05	1.29E−06	8.546E−09
b2	0.436	−4.485E−03	8.232E−05	−1.371E−06	8.776E−09
b3	0.438	−4.143E−03	7.074E−05	−1.225E−06	8.029E−09
b4	0.445	−4.264E−03	7.151E−05	−1.237E−06	8.168E−09
b5	0.491	−5.175E−03	9.576E−05	−1.613E−06	1.017E−08
b6	0.517	−4.861E−03	7.479E−05	−1.231E−06	7.787E−09
$\rho(0°/h)$ = 0.32 + (chemically treated for constant emissivity over the spectral range 8 to 12 μm)					
b1	0.348	−3.885E−03	7.636E−05	−1.050E−06	6.678E−09
b2	0.353	−3.749E−03	6.749E−05	−8.568E−07	5.263E−09
b3	0.356	−3.940E−03	7.804E−05	−1.063E−06	6.527E−09
b4	0.365	−3.994E−03	7.677E−05	−1.006E−06	5.920E−09
b5	0.390	−4.087E−03	7.774E−05	−1.056E−06	6.433E−09
b6	0.411	−4.086E−03	7.201E−05	−9.504E−07	5.885E−09
$\rho(0°/h)$ = 0.48					
b1	0.649	−5.630E−03	9.096E−05	−1.317E−06	8.376E−09
b2	0.630	−5.029E−03	8.419E−05	−1.274E−06	8.205E−09
b3	0.613	−4.680E−03	8.495E−05	−1.329E−06	8.530E−09
b4	0.605	−4.254E−03	7.711E−05	−1.170E−06	7.299E−09
b5	0.597	−3.645E−03	7.027E−05	−9.650E−07	5.311E−09
b6	0.534	−2.911E−03	5.664E−05	−6.829E−07	3.330E−09

The general equations for tarps of $\rho(0°/h)$ = 0.04, 0.08, 0.32, 0.32+ (plus emissivity treatment), and 0.48 are listed in Table 1. The general equations for tarps of $\rho(0°/h)$ = 0.08, 0.32, and 0.32+ are simply the equations derived for the one swatch that was measured (swatches labeled 0.08, 0.32a, and 0.32b). The general equations for tarps of $\rho(0°/h)$ = 0.04 and 0.48 are fourth-order equations fitted to the average of measurements for the three tarps of $\rho(0°/h)$ = 0.04 and four tarps of $\rho(0°/h)$ = 0.48, respectively, with r^2 values greater than 0.99 for all bands in both cases.

The general equations listed in Table 1 will be useful for applications with tarps of the same $\rho(0°/h)$ values as those used in this study. However, Tracor GIE offers tarps at many intermediate values of $\rho(0°/h)$, ranging from 0.02 to 0.80. Thus, it would also be useful to have a means of deriving reasonable calibration equations for tarps of any value of $\rho(0°/h)$. One approach would be to define relations between $\rho(0°/h)$ and corresponding values of the polynomial coefficients $a_{0,i}$ to $a_{4,i}$ from Equation 1.

We plotted the values of $a_{0,i}$ to $a_{4,i}$ from Table 1 for each band against the value of $\rho(0°/h)$ (Figure 3).[3] For b1 to b4, there was a logical progression of the values of the coefficients with increasing $\rho(0°/h)$ that could be fit with a second-order polynomial with r^2 values greater than 0.95. For b5 and b6, the progression of values was less reliable and required higher order polynomial fits to retain high correlation coefficients. Because there were only four values of $\rho(0°/h)$ from which to derive this relation, we felt that results from this approach were only reliable for b1 to b4. Based on the equations listed in Table 2, the coefficients $a_{0,1-4}$ to $a_{4,1-4}$ could be derived for any tarp of $0.04 < \rho(0°/h) < 0.48$. These results cannot be validated here because all the swatches were used in derivation of the equations in Table 2.

Comparison of Calibrations for Woven and Non-Woven Swatches

To compare the $\rho(0°/\theta_s)$ of the woven and non-woven swatches of the same $\rho(0°/h)$, we calibrated pairs of woven and non-woven swatches of similar $\rho(0°/h)$ values. Calibration results for four non-woven tarps are listed in Table 3. The percent difference between woven and non-woven $\rho(0°/\theta_s)$ was computed as $\Delta\% = (\rho(0°/\theta_s)_{\text{non-woven}} - \rho(0°/\theta_s)_{\text{woven}})/\rho(0°/\theta_s)_{\text{woven}} * 100$ (Figure 4).[4] In this case, if $\rho(0°/\theta_s)$ of the non-woven swatch was greater than that of the woven swatch, $\Delta\%$ would be positive. Results showed that the $\rho(0°/\theta_s)$ and non-lambertian characteristics of the woven and non-woven swatches of $\rho(0°/h)$ = 0.48 were nearly identical. The $\rho(0°/\theta_s)$ of the non-woven swatch of $\rho(0°/h)$ = 0.08 was greater than the woven swatch by up to 20 percent in b1 at large solar zenith angles. The $\rho(0°/\theta_s)$ of the non-woven swatch of $\rho(0°/h)$ = 0.04 was less than the woven swatch by up to 50 percent in b1 at small solar zenith angles. The reason for the large discrepancy between the two swatches of $\rho(0°/h)$ = 0.04 is unclear.

[3]Because of the unusual behavior of 0.32b (with emissivity treatment), it was not included in this analysis.

[4]The use of "percent difference" emphasizes the difference in the shape of the curves, but may overemphasize the magnitude of the difference. For example, a 50 percent difference for the tarp of $\rho(0°/h)$ = 0.04 would only be a difference in $\rho(0°/\theta_s)$ of 0.02, and 2 percent difference for the tarp of $\rho(0°/h)$ = 0.48 would be about 0.01.

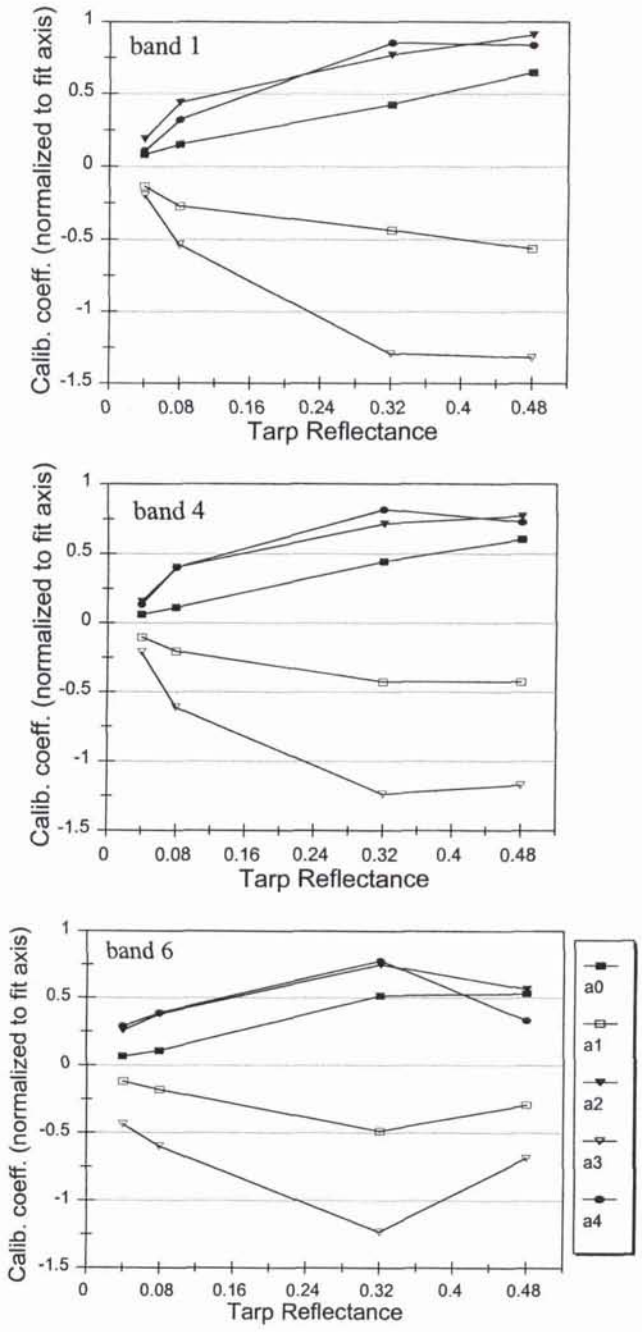

Figure 3. Relations between $\rho(0°/h)$ and corresponding values of the polynomial coefficients $a_{0,i}$ to $a_{4,i}$ from Table 1 for Equation 1 for spectral wavelength bands b1, b4, and b6. Second-order polynomial equations fit to these data are given in Table 2 for b1 to b4. Note: Because of the unusual behavior of swatch 0.32b (with the emissivity treatment), it was not included in this analysis.

TABLE 2. SECOND-ORDER POLYNOMIAL EQUATIONS RELATING THE COEFFICIENTS FROM EQUATION 1 TO $\rho(0°/h)$ FOR EACH MMR SPECTRAL BAND, b1 TO b4, WHERE $a_{n,i} = b_0 + b_1\,\rho(0°/h) + b_2\,\rho(0°/h)^2$.

Band 1	b_0	b_1	b_2	r_2
$a_{0,1}$	4.82E−02	1.10E+00	3.14E−0 1	0.998
$a_{1,1}$	−1.25E−03	−1.27E−02	7.84E−03	0.957
$a_{2,1}$	1.37E−05	3.04E−04	−3.02E−04	0.965
$a_{3,1}$	2.36E−08	−6.97E−06	8.73E−06	0.994
$a_{4,1}$	−5.71E−10	4.92E−08	−6.39E−08	0.997
Band 2				
$a_{0,2}$	2.20E−02	1.37E+00	−2.16E−01	1.000
$a_{1,2}$	−5.80E−04	−1.92E−02	2.09E−02	0.986
$a_{2,2}$	1.64E−06	4.30E−04	−5.40E−04	0.990
$a_{3,2}$	1.48E−07	−8.41E−06	1.14E−05	0.999
$a_{4,2}$	−1.06E−09	5.42E−08	−7.27E−08	0.999
Band 3				
$a_{0,3}$	5.03E−03	1.52E+00	−5.26E−01	1.000
$a_{1,3}$	−4.05E−04	−1.81E−02	1.93E−02	0.990
$a_{2,3}$	3.72E−06	3.14E−04	−3.05E−04	0.981
$a_{3,3}$	9.72E−08	−6.68E−06	7.76E−06	0.995
$a_{4,3}$	−7.29E−10	4.48E−08	−5.33E−08	0.996
Band 4				
$a_{0,4}$	−6.10E−03	1.65E+00	−7.88E−01	1.000
$a_{1,4}$	−3.27E−04	−2.12E−02	2.73E−02	0.993
$a_{2,4}$	8.74E−06	3.33E−04	−4.0 E−04	0.960
$a_{3,4}$	−2.09E−08	−6.98E−06	9.6 E−06	0.978
$a_{4,4}$	1.92E−13	4.85E−08	−6.96E−08	0.980

Tarp Temporal Degradation

Tarp Temporal Degradation With Minimal Exposure to Sunlight

During the 1997 calibration, we repeated the calibration of four woven swatches (0.04a, 0.08, 0.32b, and 0.48a) to quantify temporal swatch degradation. Jackson *et al.* (1987) reported that the precision of this goniometer-based calibration method was 1 percent, expressed as a ±0.5 percent difference from the mean $\rho(0°/\theta_s)$ of a high-reflectance target. It follows that percent differences larger than 1 percent between two calibrations of a single swatch would be due to influences other than measurement error, in this case, primarily degradation of swatch $\rho(0°/h)$. Percent differences (Δ%) were computed between the 1995 and 1997 swatch $\rho(0°/\theta_s)$, where $\Delta\% = (\rho(0°/\theta_s)_{1995} - \rho(0°/\theta_s)_{1997})/\rho(0°/\theta_s)_{1997} * 100$ (Figure 5). Thus, if swatch $\rho(0°/\theta_s)$ had decreased with time, Δ% would be positive; if swatch $\rho(0°/\theta_s)$ had increased, Δ% would be negative.

Results showed that the $\rho(0°/\theta_s)$ of swatches 0.04a and 0.08 increased for small solar zenith angles and decreased for larger solar zenith angles (>45°) for bands b1 to b4. This analysis did not include MMR bands b5 and b6 because of failure of the MMR SWIR detectors in the 1997 calibration. For all zenith angles, the $\rho(0°/\theta_s)$ of swatches 0.32b and 0.48a decreased, though the decrease was less than 8 percent. These results are compatible with the Tracor GIE assertion that "target areas higher than $\rho(0°/h) = 0.16$ tend to decrease [when exposed to sunlight and weathering] and areas lower than $\rho(0°/h) = 0.16$ tend to increase." Because our tarps had minimal exposure to both sunlight and weathering, the Δ% reported in Figure 5 represent the minimal rates of chemical degradation with time, with consideration for the precision of the calibration method (1 percent).

Tarp Temporal Degradation under Normal Field Conditions

The analysis of the R21 tarps allowed us to confirm that the *shape* of the relation between tarp $\rho(0°/\theta_s)$ and solar zenith angle was robust and could be applied to other tarps that had not been subjected to goniometer measurements. We found that the $\rho(0°/\theta_s)$ of the clean tarps followed the shape of the goniometer-derived curves within 0.01 $\rho(0°/\theta_s)$ at the three solar zenith angles measured (e.g., R21 tarp set #4 in Figure 6). For the dirty tarps, the shape was sometimes distorted, but it generally followed the goniometer-derived shape.

The visual, qualitative assessment of tarp dirtiness was used to explain the great variation in absolute measurements of $\rho(0°/\theta_s)$ of the R21 tarps of the same $\rho(0°/h)$. The tarps that were rated clean corresponded well with the $\rho(0°/\theta_s)$ determined by the goniometer-derived calibration equations for the

TABLE 3. COEFFICIENTS FOR THE POLYNOMIAL EQUATIONS RELATING $\rho(0°/\theta_s)$ AND θ_s FOR NON-WOVEN SWATCHES OF $\rho(0°/h)$ = 0.04, 0.08, 0.48, AND 0.64, WHERE $\rho(0°/\theta_s) = a_{0,i} + a_{1,i}\,\theta_s + a_{2,i}\,\theta_s^2 + a_{3,i}\,\theta_s^3 + a4_{,i}\,\theta_s^4$ AND i IS THE MMR SPECTRAL BAND b1 TO b4.

	$a_{0,i}$	$a_{1,i}$	$a_{2,i}$	$a_{3,i}$	$a_{4,i}$
$\rho(0°/h)$ = 0.04					
b1	2.866E−02	1.360E−04	−1.038E−05	2.192E−07	−1.321E−09
b2	2.800E−02	1.733E−04	−1.147E−05	2.327E−07	−1.377E−09
b3	2.880E−02	1.631E−04	−1.224E−05	2.541E−07	−1.519E−09
b4	2.723E−02	3.083E−04	−1.789E−05	3.563E−07	−2.160E−09
$\rho(0°/h)$ = 0.08					
b1	0.155	−2.626E−03	4.940E−05	−5.627E−07	2.734E−09
b2	0.136	−1.912E−03	3.085E−05	−3.049E−07	1.351E−09
b3	0.121	−1.692E−03	2.944E−05	−3.220E−07	1.617E−09
b4	0.105	−1.067E−03	7.626E−06	2.994E−08	−3.80 E−10
$\rho(0°/h)$ = 0.48					
b1	0.691	−6.558E−03	1.378E−04	−2.303E−06	1.441E−08
b2	0.662	−5.806E−03	1.261E−04	−2.176E−06	1.382E−08
b3	0.639	−5.588E−03	1.295E−04	−2.226E−06	1.402E−08
b4	0.615	−4.693E−03	1.034E−04	−1.779E−06	1.310E−08
$\rho(0°/h)$ = 0.64					
b1	0.853	−5.590E−03	1.188E−04	−2.075E−06	1.212E−08
b2	0.826	−4.780E−03	1.023E−04	−1.861E−06	1.098E−08
b3	0.812	−5.136E−03	1.259E−04	−2.230E−06	1.291E−08
b4	0.788	−3.797E−03	7.886E−05	−1.443E−06	8.328E−09

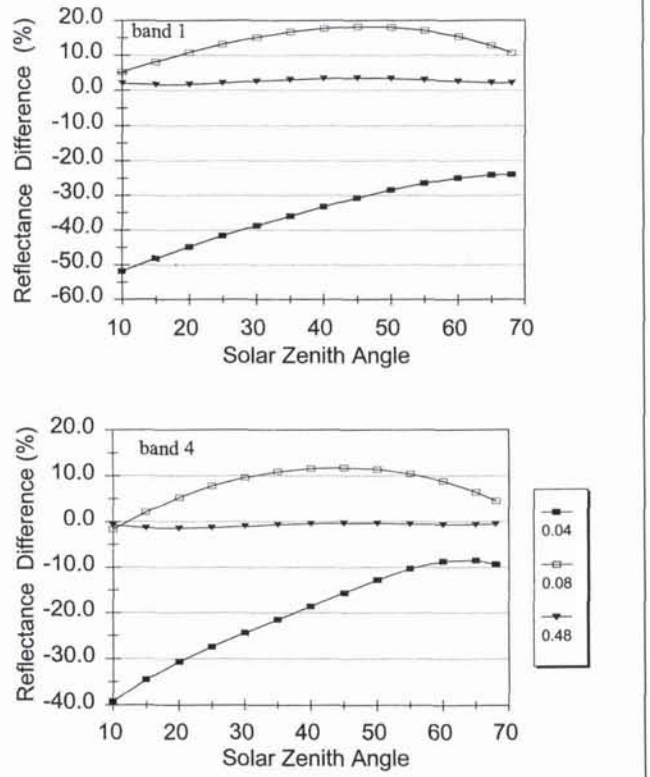

Figure 4. Percent difference (Δ%) of the $\rho(0°/\theta_s)$ of woven and non-woven swatches of the same $\rho(0°/h)$, where $\Delta\% = (\rho(0°/\theta_s)_{\text{non-woven}} - \rho(0°/\theta_s)_{\text{woven}})/\rho(0°/\theta_s)_{\text{woven}} * 100$. If $\rho(0°/\theta_s)$ of the non-woven swatch was greater than that of the woven swatch, Δ% would be positive.

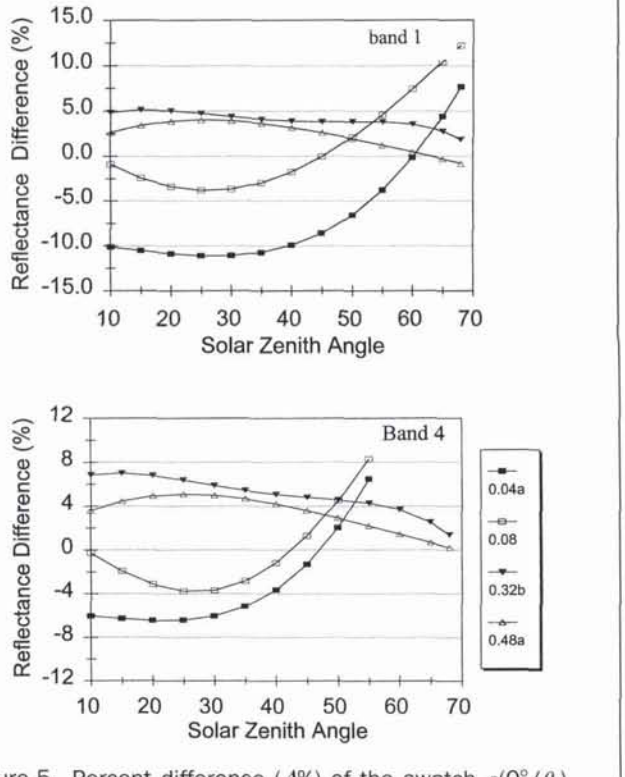

Figure 5. Percent difference (Δ%) of the swatch $\rho(0°/\theta_s)$ measured in 1995 and 1997 for swatches 0.04a, 0.08, 0.32b, and 0.48a, where $\Delta\% = (\rho(0°/\theta_s)_{1995} - \rho(0°/\theta_s)_{1997})/\rho(0°/\theta_s)_{1997} * 100$. If the swatch $\rho(0°/\theta_s)$ had decreased with time, Δ% would be positive.

swatches (Figure 7). Though this was a subjective dirtiness classification, the results implied that the deviation of the field measurements of $\rho(0°/\theta_s)$ from the goniometer-derived $\rho(0°/\theta_s)$ was a function of tarp dirtiness. Furthermore, the direction of the deviation depended upon the tarp $\rho(0°/h)$. That is, as the tarps of $\rho(0°/h)$ = 0.04 and $\rho(0°/h)$ = 0.08 became dirtier, the field measurements of $\rho(0°/\theta_s)$ tended to increase, and as the tarps of $\rho(0°/h)$ = 0.48 and $\rho(0°/h)$ = 0.64 became dirtier, the field measurements of $\rho(0°/\theta_s)$ decreased.

These qualitative results were confirmed by the results of the experiment conducted on the goniometer with tarp swatches at different stages of dirtiness (Figure 8). Recall from the description in the Materials and Methods Section, that we created "dirty" tarp swatches by dumping a handful of soil on each swatch, rubbing it gently into the swatch, and brushing

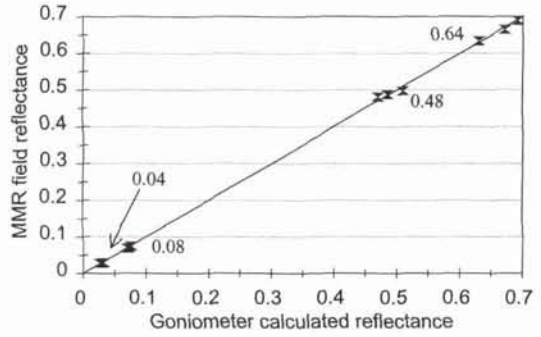

Figure 6. Comparison of $\rho(0°/\theta_s)$ of several clean tarps measured with the MMR and the goniometer-derived tarp ($\rho(0°/\theta_s)$) for three solar zenith angles for spectral wavelength band b4.

off the soil particles with a cotton cloth. The percent difference in $\rho(0°/\theta_s)$ ($\%\Delta\rho$) was computed by taking the difference between $\rho(0°/\theta_s)$ of the dirty and clean swatches, dividing it by $\rho(0°/\theta_s)$ of the clean tarp, and multiplying by 100. This $\%\Delta\rho$ was as high as 70 percent in b4 for tarps of $\rho(0°/h) = 0.04$, and as high as 15 percent in b1 for tarps of $\rho(0°/h) = 0.64$.

We also used these goniometer data to investigate the effect of dirtiness on the shape of the relation between swatch $\rho(0°/\theta_s)$ and solar zenith angle. We found that the shape was *slightly* distorted with tarp dirtiness, but only at very large θ_s (>50°). These results are evident in the small standard deviations of the average of measurements over the large range of θ_s (Figure 8). This gave support to the assumption that the shape of this relation was relatively robust.

Tarp Calibration Related to θ_v

As described in the methods section, the directional/directional reflectance factor ($\rho(\theta_v/\theta_s)$) was measured for tarps of $\rho(0°/h) = 0.04$, 0.08, 0.48, and 0.64 at two solar zenith angles, three scanning planes, and θ_v ranging from +55° to −55°. These $\rho(\theta_v/\theta_s)$ measurements are illustrated in Figure 9 for a solar angle of 47°. The data are organized into two columns, where the left column illustrates data scanned in the principal plane (PP), and the right column illustrates data acquired in a plane 45° off the principle plane. For tarps of $\rho(0°/h) \geq 0.08$, the measurements of tarp $\rho(\theta_v/\theta_s)$ were considerably higher in the backscattering direction, when the sun and sensor were aligned in the same azimuthal hemisphere and shadows were

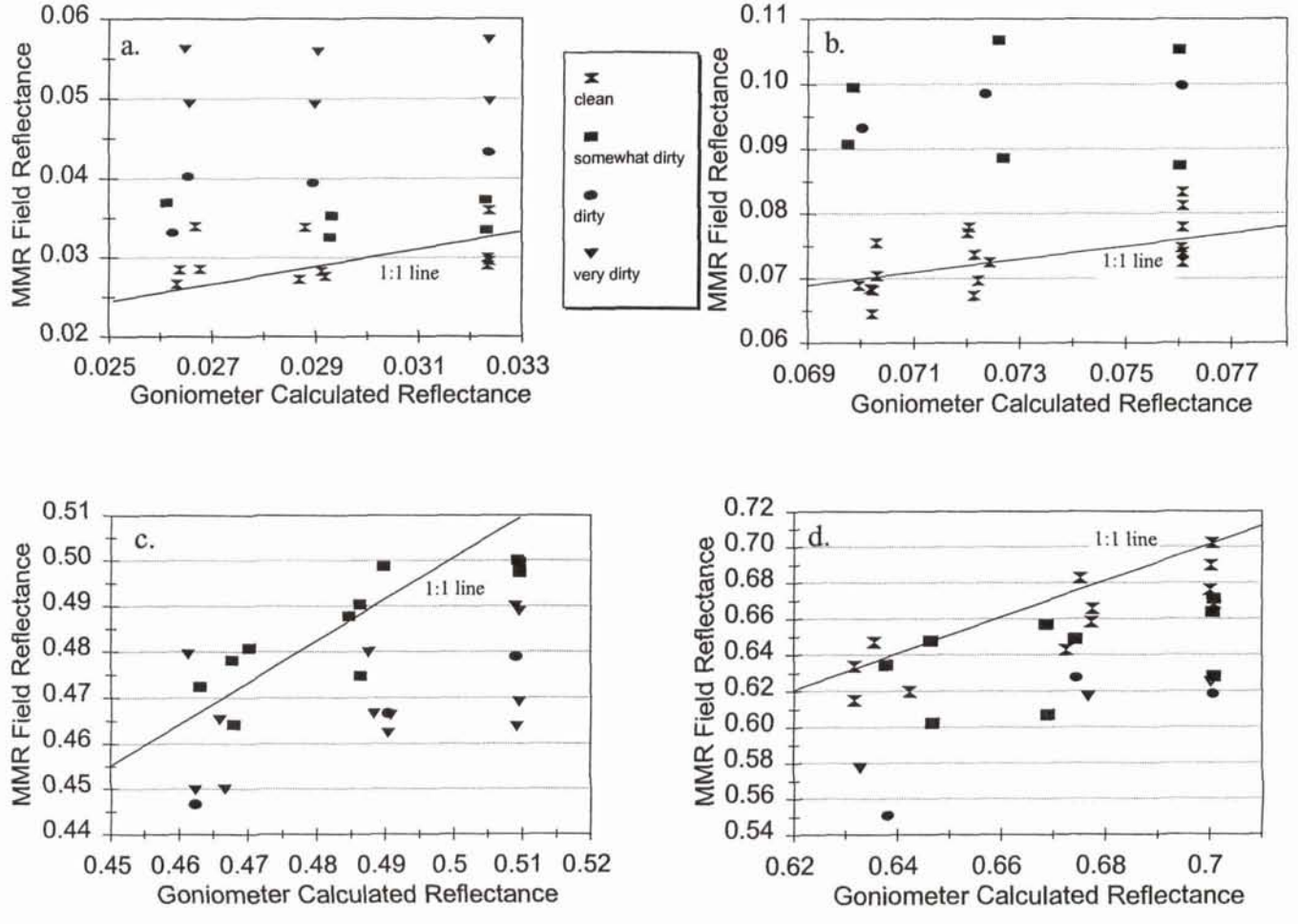

Figure 7. Comparison of the MMR measurements of tarp $\rho(0°/\theta_s)$ with the goniometer-derived tarp $\rho(0°/\theta_s)$ for tarps of $\rho(0°/h)$ = (a) 0.04, (b) 0.08, (c) 0.48, and (d) 0.64. The data markers express the qualitative tarp dirtiness as determined by visual observation.

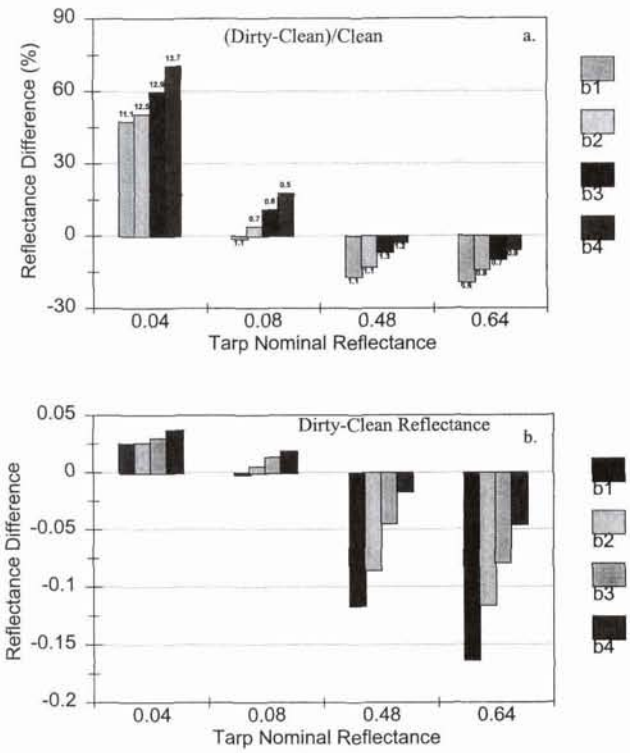

Figure 8. The difference in $\rho(0°/\theta_s)$ of dirty and clean swatches presented as (a) percent difference (where Δ% is the difference between the $\rho(0°/\theta_s)$ of the dirty and clean swatches divided by $\rho(0°/\theta_s)$ of the clean swatch, multiplied by 100) and (b) the difference between the $\rho(0°/\theta_s)$ of dirty and clean swatches. The bars are labeled with the standard deviation of the measurements made at four solar zenith angles.

minimized. The non-lambertian properties of the tarp of $\rho(0°/h) = 0.04$ were significantly different; that is, the highest $\rho(\theta_v/\theta_s)$ was measured in the forward scattering direction. This was due to strong specular reflectance from the tarp of $\rho(0°/h) = 0.04$. For the tarp of $\rho(0°/h) = 0.04$, the specular effect was much stronger than the backscatter effect. In contrast, for the tarp of $\rho(0°/h) = 0.64$, the backscatter effect was stronger than the specular effect.

For the view angles used in this study, we computed the percent difference between $\rho(\theta_v/\theta_s)$ measured at $\theta_v > 0°$ and at $\theta_v = 0°$. The variation due to view angle differences was as large as 37 percent for the tarps of $\rho(0°/h) = 0.04$ at $\theta_v = 40°$. The tarps of $\rho(0°/h) = 0.04$ and 0.08 had the largest variation while the tarp of $\rho(0°/h) = 0.64$ showed minimal view angle effects (<20 percent). The high variation for the tarps of $\rho(0°/h) = 0.04$ and 0.08 may be due to (1) low sensor signal because there was little reflected radiation, and (2) the specular effect shown in a photo taken during the experiment (Figure 10). The tarp of $\rho(0°/h) = 0.04$ was not only sensitive to the specular effect, but also to the spatial variation of the tarps due to wrinkles.

The $\rho(\theta_v/\theta_s)$ measurements were then fit to a BRDF model (Shibayama and Wiegand, 1985) to investigate how models could be used to normalize the differences due to view angle variations. The general form of the Shibayama/Wiegand model is

$$\rho(\theta_s/\theta_v) = \rho(0°/0°)\,[1 + \beta_0 + \beta_1 \sin(\varphi/2) + \beta_2/\cos\theta_s)\sin\theta_v], \qquad (2)$$

where φ is the azimuthal difference between principal planes of the sun and sensor, and β_0, β_1, and β_2 are model-derived empirical coefficients. The model-simulated values were plotted against measured $\rho(\theta_v/\theta_s)$ values in Figure 11. The model worked well for the tarps of $\rho(0°/h) = 0.48$ and 0.64, with less accurate predictions for the tarps of $\rho(0°/h) = 0.04$ and 0.08. This was partially due to the strong specular effects found for the tarp of $\rho(0°/h) = 0.04$, and to a lesser degree for the tarp of $\rho(0°/h) = 0.08$. Most BRDF models were developed for vegetated land surfaces, and do not account for specular reflectance. Nevertheless, the Shibayama and Wiegand model performed well overall. The coefficients of the model are listed in Table 4 for all tarps and all spectral bands (b1 to b4).

Discussion

From this analysis, it is apparent that there are several sources of variation in tarp $\rho(\theta_v/\theta_s)$ that must be accounted for in proper tarp deployment. These include differences in $\rho(\theta_v/\theta_s)$ due to variations in (1) initial chemical application, (2) tarp dirtiness due to field deployment, (3) θ_s, and (4) θ_v. Based on our measurements, we made reasonable, comparable determinations of the variation in $\rho(\theta_v/\theta_s)$ associated with these four phenomena (Figure 12). The results showed that the variation in tarp $\rho(\theta_v/\theta_s)$ due to differences in initial Tracor GIE chemical application (computed by comparing $\rho(\theta_v/\theta_s)$ of multiple clean tarps and swatches) was relatively small, with an average variation close to zero and a maximum variation of 20 percent for tarps of $\rho(0°/h) = 0.04$ in the NIR spectrum (b4). The effects of dirtiness could be quite large (resulting in up to 50 percent variation in $\rho(\theta_v/\theta_s)$). The effects of θ_s and θ_v at operational values ($\theta_s = 45°$ and $\theta_v = 40°$) can exceed the effects of dirtiness, particularly for tarps of $\rho(0°/h) = 0.48$ and 0.64.

It should be apparent from results presented in Figure 12 that the total error associated with tarp deployment for image calibration could potentially be quite large. On the other hand, if tarps are deployed correctly and kept clean through careful use and periodic cleaning, and if tarp $\rho(\theta_v/\theta_s)$ is determined through calibration equations that account for both θ_s and θ_v, the greatest sources of error will be minimized.

Conclusions

Based on the analysis of swatches of tarps, we made the following conclusions related to the use of large reference tarps under field conditions. We found that tarp non-lambertian properties were substantial for all values of $\rho(0°/h)$, and that these properties varied by both the spectral band and the value of $\rho(0°/h)$. It appeared that tarps could be used with some confidence in the visible and NIR spectral range, but care should be taken when making measurements in SWIR spectral bands because the behavior was less predictable. Furthermore, the chemical treatment used by Tracor GIE to induce constant emissivity properties affected the $\rho(0°/\theta_s)$ of the tarp and resulted in a unique calibration equation.

General calibration equations were derived with some confidence for spectral bands b1 to b6, for woven tarps of the $\rho(0°/h)$ values measured in this study (Table 1). Equations were also provided to allow a calibration equation to be determined from the value of $\rho(0°/h)$ for the spectral bands b1 to b4, limited to woven tarps of $0.04 < \rho(0°/h) < 0.48$ (Table 2).

The characteristics of the woven and non-woven materials were compared by calibration of swatches from woven and non-woven tarps of $\rho(0°/h) = 0.04$, 0.08, and 0.48. For tarps of $\rho(0°/h) = 0.48$, the $\rho(0°/\theta_s)$ and non-lambertian properties of woven and non-woven materials were nearly identical. For $\rho(0°/h) = 0.04$ and 0.08, woven and non-woven materials differed in both $\rho(0°/\theta_s)$ and non-lambertian behavior by up to 50 percent of $\rho(0°/\theta_s)$.

A limited test was conducted to determine the degradation of the tarp $\rho(0°/\theta_s)$ properties with time, under conditions of minimal exposure to sunlight and weathering. The tarp $\rho(0°/\theta_s)$

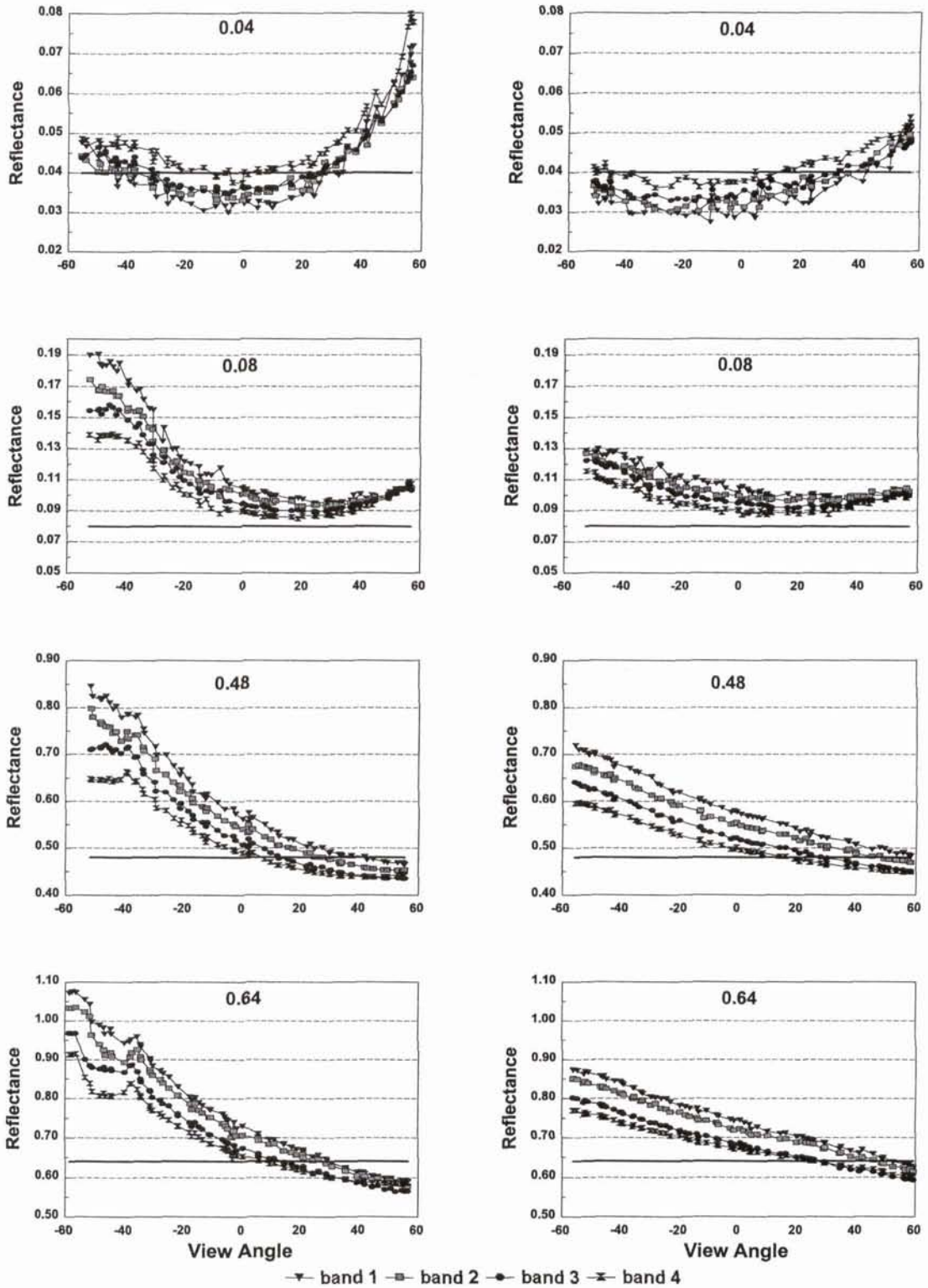

Figure 9. The non-lambertian properties of tarps of ($\rho(0°/h)$ = 0.04, 0.08, 0.48, and 0.64) at solar zenith angle 47°. The left column illustrates data scanned in the principal plane (PP) and the right column illustrates data acquired at 45° off PP.

increased for the low-reflectance tarps ($\rho(0°/h) < 0.16$) and decreased for the tarps of $\rho(0°/h) > 0.16$ by as much as 10 percent of $\rho(0°/\theta_s)$ in some cases. In units of $\rho(0°/\theta_s)$, results showed a maximum increase of about 0.004 for the tarp of $\rho(0°/h) = 0.04$ and a maximum decrease of about 0.02 for the tarp of $\rho(0°/h) = 0.48$.

Our measurements of the 36 tarps that were deployed by R21 during the 1997 field season showed that the tarps varied

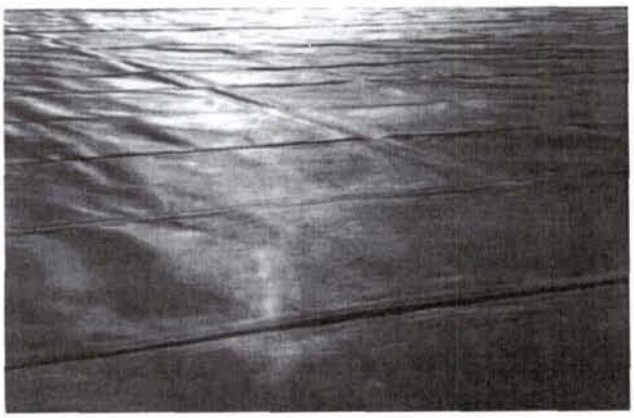

Figure 10. Photograph illustrating the strong specular effect for tarps of $\rho(0°/h) = 0.04$. This photograph was taken at a solar zenith angle of 68° viewing to the east (toward the sun).

TABLE 4. COEFFICIENTS FOR EVALUATION OF EQUATION 2 DERIVED FROM INVERSION OF THE SHIBAYAMA AND WIEGAND BRDF MODEL, $\rho(\theta_s/\theta_v) = \rho_0 [1 + \beta_0 + \beta_1 \sin(\varphi/2) + \beta_2/\cos\theta_s)\sin\theta_v]$. COEFFICIENTS ARE LISTED BY MMR SPECTRAL BANDS, b1 TO b4.

Coefficients	b1	b2	b3	b4
		$\rho(0°/h) = 0.04$		
ρ_0	0.0302	0.0306	0.0340	0.0376
β_0	0.2336	1.3463	0.2046	0.5521
β_1	0.2415	0.4083	0.2298	0.2489
β_2	0.0506	−0.6886	−0.0051	−0.2301
		$\rho(0°/h) = 0.08$		
ρ_0	0.0983	0.0922	0.0888	0.0836
β_0	1.1617	1.2993	1.0435	0.8226
β_1	−0.8310	−0.7442	−0.6489	−0.5007
β_2	−0.2233	−0.3225	−0.1966	−0.0969
		$\rho(0°/h) = 0.48$		
ρ_0	0.5552	0.5298	0.5011	0.4809
β_0	0.9094	0.8963	0.8801	0.7151
β_1	−0.7998	−0.7681	−0.7339	−0.6295
β_2	−0.2007	−0.2001	−0.2020	−0.1369
		$\rho(0°/h) = 0.64$		
ρ_0	0.7143	0.6916	0.6594	0.6474
β_0	0.7908	0.8742	0.7462	0.6159
β_1	−0.6688	−0.6389	−0.6069	−0.5031
β_2	−0.1920	−0.2478	−0.1836	−0.1415

in $\rho(0°/\theta_s)$. We postulate that this was due to a combination of the variations in the initial chemical application and the current state of tarp dirtiness due to field deployment. The shape of the relation between $\rho(0°/\theta_s)$ and θ_s was consistent for swatches of similar $\rho(0°/h)$. This shape was slightly distorted with tarp dirtiness at $\theta_s > 50°$, and tarp dirtiness had a substantial effect on tarp $\rho(0°/\theta_s)$. Increasing dirtiness caused $\rho(0°/\theta_s)$ to increase for tarps of $\rho(0°/h) = 0.04$ and 0.08; it caused $\rho(0°/\theta_s)$ to decrease for tarps of $\rho(0°/h) = 0.48$ and 0.64. The calibration equations for clean tarps were not substantially different from the calibration equations derived for clean swatches using the goniometer.

All tarps had strong sensitivity to θ_v, resulting in percent $\rho(\theta_v/\theta_s)$ differences up to 37 percent for a sensor view angle of 40°. Unexpected strong specular effect was found for the tarp of $\rho(0°/h) = 0.04$, resulting in poor model prediction. Because most BRDF models were developed for natural land surface, the

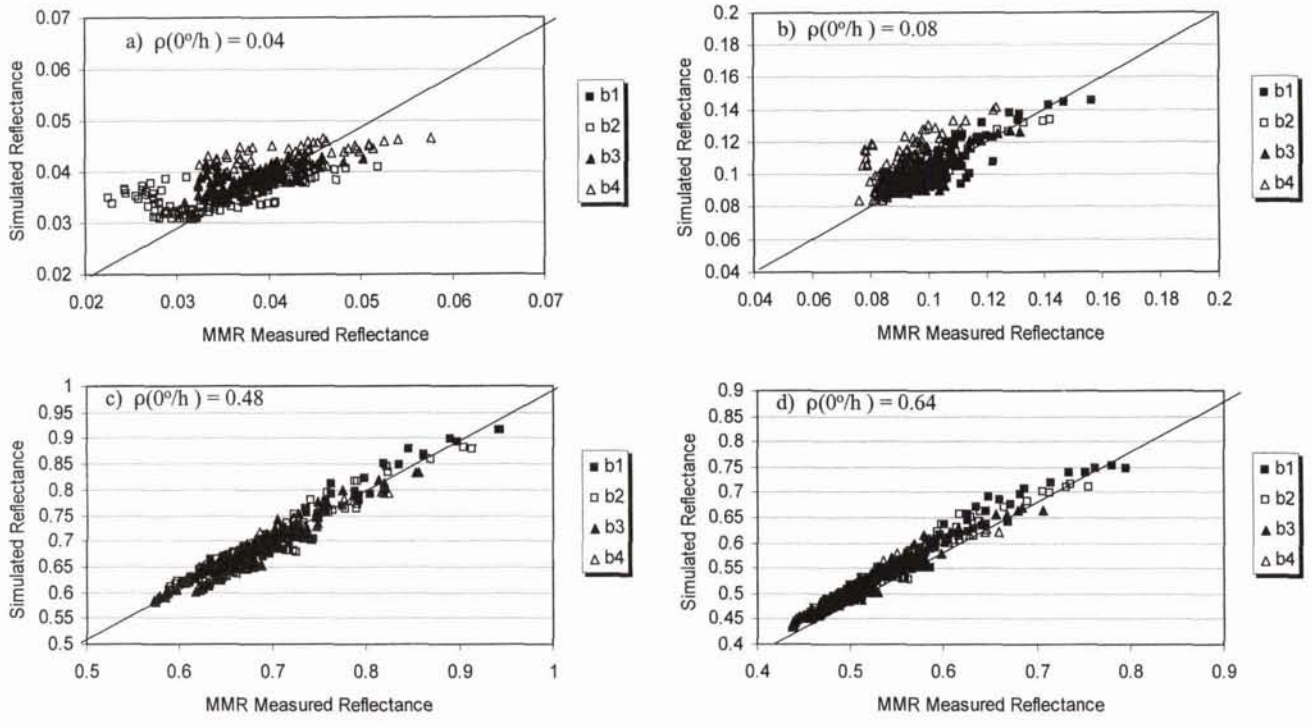

Figure 11. Comparison of model-derived values of $\rho(\theta_v/\theta_s)$ for tarps of $\rho(0°/h)$ (a) 0.04, (b) 0.08, (c) 0.48, and (d) 0.64 for wavelength spectral bands b1 to b4 at a variety of view angles with measured $\rho(\theta_v/\theta_s)$ using the Exotech radiometer mounted on a movable boom.

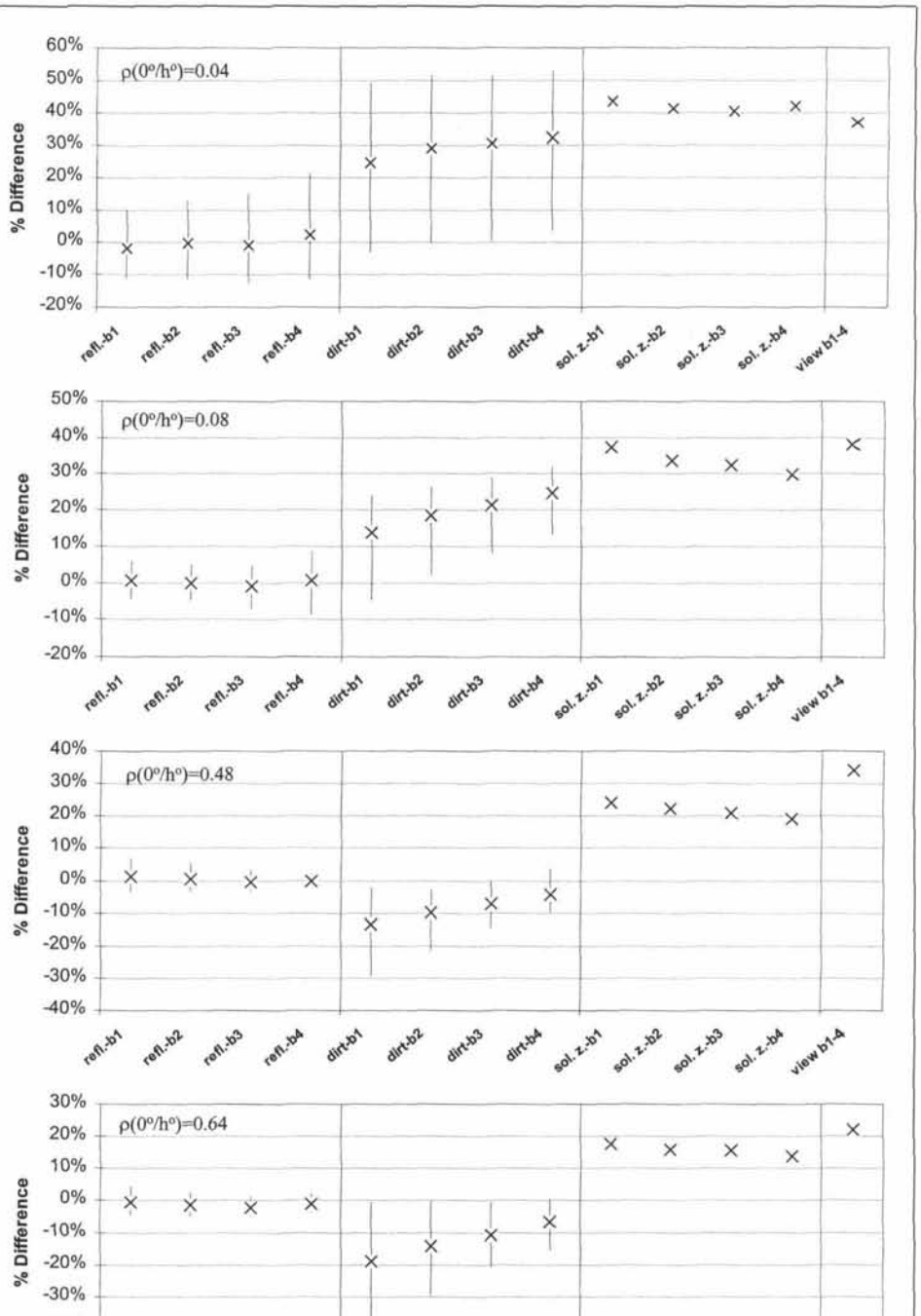

Figure 12. Percent difference in measurement of $\rho(\theta_v/\theta_s)$ for tarps of $\rho(0°/h) = 0.04$, 0.08, 0.48, and 0.64. The *x*-axis labels are defined as follows: *refl* = percent difference between $\rho(\theta_v/\theta_s)$ measured of clean tarps in the field and $\rho(\theta_v/\theta_s)$ calculated from goniometer measurements; *dirt* = percent difference between measured $\rho(\theta_v/\theta_s)$ of dirty tarps and $\rho(\theta_v/\theta_s)$ calculated from goniometer measurements; *sol. z.* = maximum percent difference between $\rho(\theta_v/\theta_s)$ calculated from goniometer measurements at solar zenith angles of 0° and 45°; and *view* = maximum percent difference between $\rho(\theta_v/\theta_s)$ measured at view angles of 0° and 45° at several solar zenith angles. The symbol × is the average (for *refl* and *dirt*) or maximum (for *sol. z.* and *view*) of all measurements, and vertical bars represent the range of maximum to minimum percent differences.

BRDF of the low-reflectance tarps was poorly predicted. On the other hand, the BRDF of tarps of $\rho(0°/h) = 0.08$, 0.48, and 0.64 was predicted well with the Shibayama and Wiegand model. It is thus desirable to modify one of the BRDF models to specifically include the specular effect.

On the whole, when tarps are calibrated for variations in θ_s and θ_v and kept clean through careful use and periodic cleaning, tarps can provide a means of aircraft-based image correction that is both accurate and operational. However, the logistics of tarp deployment can be problematic at times. First, tarps of this size are heavy (up to 45 kg including the container weight) and cumbersome, and deployment requires the time and effort of several persons before and after the aircraft overpass. Second, it takes some effort to keep the tarps clean, despite dusty and muddy field conditions. Third, tarps of this size are very sensitive to windy conditions. The woven tarps can quickly become unmanageable, and the non-woven tarps are easily torn under even moderate wind conditions.

Further work could be conducted to clarify tarp properties related to two points: degradation with time and differences between $\rho(\theta_v/\theta_s)$ of woven and non-woven materials. These two issues were addressed in this study, but results were inconclusive. To address the degradation of tarp $\rho(\theta_v/\theta_s)$ with time, we propose to expose the board-mounted swatches to measured amounts of sunlight, and then repeat the goniometer-based calibration procedure. To address the apparent difference in the $\rho(\theta_v/\theta_s)$ of woven and non-woven materials, we will need to obtain more swatches from Tracor GIE to validate our initial results.

Acknowledgments

Thanks to all scientists at ARS laboratories and Universities that cooperated in the purchase of these tarps; thanks to Ric Rokey, Suzette Gerszewski, Michael Helfert, and Ed Barnes for assisting in the goniometer measurements; and thanks to John Clyde and Bill Wallace of Tracor GIE for providing the calibration swatches. We appreciated the efforts of scientists at RESOURCE21 to provide field tarps, personnel, and radiometric equipment for several calibration efforts. We also thank Norman O'Neill (University of Sherbrooke) and Philip Teillet (Canada Remote Sensing Centre) for loaning us the first tarps in 1994 and encouraging us to conduct this analysis.

References

Hsia, J.J., and V.R. Weidner, 1981. NBS 45° normal reflectometer for absolute reflectance factors, *Metro*, 17:97–102.

Jackson, R.D., M.S. Moran, P.N. Slater, and S.F. Biggar, 1987. Field calibration of reference reflectance panels, *Remote Sensing of Environment*, 22:145–158.

Jackson, R.D., P.M. Teillet, P.N. Slater, G. Fedosejevs, M.F. Jasinski, J.K. Aase, and M.S. Moran, 1990. Bidirectional measurements of surface reflectance for view angle corrections of oblique imagery, *Remote Sensing of Environment*, 32:189–202.

Jackson, R.D., T.R. Clarke, and M.S. Moran, 1992. Bidirectional calibration results for 11 Spectralon and 16 BaS04 reference reflectance panels, *Remote Sensing of Environment*, 40:231–239.

Moran, M.S., T.R. Clarke, J. Qi, and P.J. Pinter, Jr., 1996. MADMAC: A test of multispectral airborne imagery as a farm management tool, *Proceedings, 26th International Symposium on Remote Sensing of Environment*, 25–29 March, Vancouver, B.C., Canada, pp. 612–617.

Neale, C.M., J. Qi, M.S. Moran, P.J. Pinter, Jr., T.R. Clarke, T.A. Mitchell, B. Crowther, S. Sundararam, and R. Ahmed, 1995. Methods of radiometric calibration and reflectance determination from airborne multispectral digital video imagery, *Proceedings 15th Bienniel Workshop on Color Photography. and Videography in Res. Assessment*, 01-01 May, Terre Haute, Indiana, pp. 87–99.

O'Neill, N.T., F. Zagolski, M. Bergeron, A. Royer, J.R. Miller, and J. Freemantle, 1997. Atmospheric correction validation of CASI images acquired over the BOREAS southern study area, *Canadian Journal of Remote Sensing*, 23:143–162.

Shibayama, M., and C.L. Wiegand, 1985. View azimuth and zenith, and solar angle effects using spectral albedo-based vegetation indices, *Remote Sensing of Environment*, 18:91–103.

Teillet, P.M., P.N. Slater, R.D. Jackson, G. Fedosejevs, and M.S. Moran, 1987. Reflectance measurements at White Sands, New Mexico, using a mobile spectroscopy laboratory, *Proceedings 11th Canadian Symposium on Remote Sensing*, 22–25 June, Waterloo, Ontario, Canada, pp. 441–450.

Walter-Shea, E.A., and L.L. Biehl, 1990. Measuring vegetation spectral properties, *Remote Sensing Review*, 5:179–205.

Walter-Shea, E.A., C.J. Hays, M.A. Mesarch, and R.D. Jackson, 1993. An improved goniometer system for calibrating field reference-reflectance panels, *Remote Sensing of Environmemt*, 43:131–138.

Zerlaut, G.A., and T.E. Anderson, 1981. Multiple-integrating sphere spectrophotometer for measuring absolute spectral reflectance and transmittance, *Applied Optics*, 20:3797–3804.

(Received 01 October 1999; revised and accepted 27 February 2000)